

Mesoscopic superfluid to superconductor transition

Yehoshua Winsten, Doron Cohen

Department of Physics, Ben-Gurion University of the Negev, Beer-Sheva 84105, Israel

Spectrum tomography for the energy (E) of a ring-shaped Bose-Hubbard circuit is illustrated. There is an inter-particle interaction U that controls superfluidity (SF) and the transition to the Mott Insulator (MI) regime. The circuit is coupled to an electromagnetic cavity mode of frequency ω_0 , and the coupling is characterized by a generalized fine-structure-constant α that controls the emergence of superconductivity (SC). The (U, α, ω_0, E) diagram features SF and SC regions, a vast region of fragmented possibly chaotic states, and an MI regime for large U . The mesoscopic version of the Meissner effect and the Anderson-Higgs mechanism are discussed.

I. INTRODUCTION

The superfluid (SF) to Mott insulator (MI) transition in the Bose-Hubbard (BH) model stands out as a paradigmatic example for quantum phase transitions [1–4]. It provides a simplified description of interacting bosonic particles confined in a lattice potential. In the SF regime one observes that the system can have both metastable condensates and fragmented (FR) states. The former support SF, while the latter are accessible once the system thermalizes. Closely related is superconductivity (SC) [5, 6]. The theory of SC has two faces: On the one hand we have the BCS theory that clarifies why electrons behave in some sense as a bosons, due to Cooper pairing. The other aspect is the Meissner effect, which is related to the interaction with the electromagnetic (EM) field, and to the Anderson-Higgs mechanism [7–10]. It is the latter aspect that makes the notion of SC distinct from SF.

Minimal model for SF.— The BH model serves as a minimal model for the explanation of SF. Namely, the superflow becomes metastable thanks to the inter-particle interactions. But if the interaction is further increased, the ground state changes from coherent condensation, to a fragmented site-occupation, which is the SF-MI transition [11–13]. Formally speaking, this transition is abrupt only for an infinite chain, but its mesoscopic version is clearly apparent even for the two-site model, as pointed out long ago by Leggett [1], who called it a transition from Josephson-regime to Fock-regime [14, 15]. For a ring with several sites, condensation in an excited momentum orbital implies the feasibility of superflow. Additionally, one has to address the significance of the underlying *chaos*. Recent studies of the chaos-mediated SF-MI transition are [16, 17] and [18]. The latter adopts a *tomographic approach* that we would like to pursue.

Minimal model for SC.— The question arises, what is the minimal model for the discussion of the SF-SC-MI transition and the Meissner effect. We take here literally the old idea that SC can be regarded as arising from condensation of charged bosons. Accordingly, the minimal model consists of a BH ring coupled to a single EM mode of a cavity. The latter is modeled as an LC oscillator. This configuration is enough to demonstrate the emergence of SC. The dimensionless parameter that char-

acterizes the coupling between the BH ring and the EM mode is a dimensional fine structure constant α . This parameter controls the crossover from the SF regime to an SC regime. The excitation frequencies of the system are affected by this EM interaction, which constitutes a mesoscopic version of the Anderson-Higgs mechanism. On top we have the inter-particle interaction that can induce a transition to an MI regime.

Quantum chaos.— The SF-MI transition is apparent also in the parametric evolution of the *excited states*. In this context, quantum chaos is an aspect that should not be overlooked [16, 17, 19–26]. The common “quantum chaos” practice to characterize a system is to look on its energy level statistics. But such approach has two issues: (i) It provides numerically clear results only for rather simple systems with large number (N) of particles, such that the spectrum in the range of interest is dense enough; (ii) It does not allow classification of the eigenstates in the typical situation of underlying mixed chaotic and quasi-regular dynamics. In the present context, one would like to highlight meta-stable SF states that are embedded in a background of FR states.

Tomography.— As opposed to the common practice, our approach is *numerically cheap* and flexible enough to deal with small complex systems. We use the term *quantum phase-space tomography* [18] in order to emphasize that the inspection of the spectrum is not limited to “level statistics”, neither focused on the ground state, and possibly reveals the relation to the underlying phase space structure. The latter serves as a classical skeleton for the quantum eigenstates.

Outline.— The circuit Hamiltonian and its parameters are introduced in Sec. (II) and Sec. (III). The big picture regarding SF/SC superflow is provided in Sec. (IV). The topography of the energy landscape is discussed in Sec. (V), with focus on the Landau perspective. The semiclassical SF-SC border is explained in Sec. (VI). Tomography measures are defined in Sec. (VII) and applied in Sec. (VIII). The various regions in the quantum spectrum are further elaborated in Sec. (IX). The mesoscopic Meissner effect and its relation to the Anderson-Higgs mechanism are discussed in Sec. (X). We finalize with a summary in Sec. (XI). The extra appendices Appendix A and Appendix B and Appendix C help to place this work in the common context of SC studies.

II. THE MODEL

We consider a circuit that is modeled as a Bose-Hubbard ring that interacts with a cavity mode. The EM mode is described by conjugate variables (Q, Φ) that essentially encodes the electric field and the magnetic flux, see [Appendix A](#). The dynamics of the bosons on the ring is generated by operators \mathbf{a}_j and \mathbf{a}_j^\dagger that annihilate and create particles in sites that are indexed by j . Additionally, in Coulomb gauge, the Hamiltonian contains also a term \mathcal{U}_{ES} for the extra electrostatic energy.

$$\mathcal{H} = \frac{U}{2} \sum_j \mathbf{a}_j^\dagger \mathbf{a}_j^\dagger \mathbf{a}_j \mathbf{a}_j - \frac{K}{2} \sum_{j=1}^L \left[\mathbf{a}_{j+1}^\dagger \mathbf{a}_j e^{i(1/L)e\Phi} + \text{hc} \right] + \mathcal{U}_{ES} + \frac{c^2}{2L_e} \Phi^2 + \frac{1}{2C_e} Q^2 \quad (1)$$

where L_e and C_e have dimension of length, and reflect the geometry of the system. In particular, the bare frequency of the EM-mode reflects the linear size \mathcal{R} of the cavity

$$\omega_0 = \frac{c}{\sqrt{L_e C_e}} \equiv \frac{c}{\mathcal{R}} \quad (2)$$

As explained in [Appendix A](#), typically $L_e \sim \mathcal{L}^2/\mathcal{R}$, where \mathcal{L} is the linear size of the ring. We choose convenient units of charge

$$q^2 = \sqrt{\frac{C_e}{L_e}} c \quad (3)$$

and define

$$\mathbf{b} = \frac{1}{\sqrt{2}} \left[q\Phi + \frac{i}{q} Q \right] \quad (4)$$

The dimensionless flux is

$$\phi = e\Phi = \sqrt{\frac{\alpha}{2}} (\mathbf{b}^\dagger + \mathbf{b}) \quad (5)$$

where the generalized fine structure constant is

$$\alpha \equiv \frac{e^2}{q^2} \sim \frac{e^2}{c} \left(\frac{\mathcal{L}}{\mathcal{R}} \right)^2 \quad (6)$$

The Hamiltonian takes the form

$$\mathcal{H} = \omega_0 \mathbf{b}^\dagger \mathbf{b} + \frac{U}{2} \sum_j \mathbf{a}_j^\dagger \mathbf{a}_j^\dagger \mathbf{a}_j \mathbf{a}_j + \mathcal{U}_{ES} - \frac{K}{2} \sum_{j=1}^L \left[\mathbf{a}_{j+1}^\dagger \mathbf{a}_j e^{i(1/L)\sqrt{\frac{\alpha}{2}}(\mathbf{b}^\dagger + \mathbf{b})} + \text{hc} \right] \quad (7)$$

The explicit expression for the extra electrostatic energy \mathcal{U}_{ES} of [Eq.\(A4\)](#) as a function of the occupation operators $\mathbf{a}_j^\dagger \mathbf{a}_j$ will be provided in a later section.

We switch to the momentum representation:

$$\mathcal{H} = \frac{\omega_0}{2} \left[\frac{\alpha}{2} \mathbf{n}_{osc}^2 + \frac{2}{\alpha} \phi^2 \right] - K \sum_k \mathbf{n}_k \cos \left(k - \frac{\phi}{L} \right) + \mathcal{U}_{ES} - \frac{U}{2L} \sum_k \mathbf{n}_k^2 + \text{transitions} \quad (8)$$

where $\mathbf{n}_{osc} = (1/e)Q$, and \mathbf{n}_k are the occupations of the momentum orbitals. The latter are indexed by

$$k = k_m = \frac{2\pi}{L} m, \quad [m = \text{integer mod}(L)] \quad (9)$$

The trimer ($L=3$) has three orbitals that we label as k_0 and k_{\pm} . In the numerical code the standard basis consists of the occupation states $|n_k, n_{osc}\rangle$. These are the eigenstates of the $U=0$ Hamiltonian. Condensation in the k_m orbital means $n_k = N\delta_{k,k_m}$.

III. MODEL PARAMETERS

The parameters ($L, N, N_{osc}, K, U, \omega_0, \alpha$) define the Hamiltonian [Eq.\(7\)](#), where N_{osc} is an insignificant arbitrary numerical truncation of the oscillator's Hilbert space for numerical purpose. We want to define set of dimensionless parameters that appear in the *classical* equations of motion. For the ring the scaled coordinates are $\tilde{\mathbf{a}}_j = \mathbf{a}_j/\sqrt{N}$, while for the oscillator we keep ϕ and define consistently $\tilde{\mathbf{q}} = \mathbf{q}/N$, such that $\hbar_{scaled} = 1/N$ for all the canonical coordinates. Consequently, the implied classical Hamiltonian is $H_{cl} = \mathcal{H}/N$. Without loss of generality we choose the units of time such that $K=1$. Accordingly the *classical* dimensionless parameters are

$$\left(u \equiv \frac{NU}{K}, \omega_0/K, N\alpha \right) \quad (10)$$

Additionally, we have to specify the number of sites L . Assuming a large multi-site ring $L \gg 1$, with lattice spacing ℓ , We can define effective Gross-Pitaevskii Equation (GPE) parameters, namely, the mass $M = 1/(K\ell^2)$, the interaction $g = \ell U$, and the length $\mathcal{L} = L\ell$. It is convenient to define dimensionless parameters that survive the continuum limit, such that the dependence on ℓ cancels out. These are

$$u_L = L \frac{NU}{K} = \mathcal{L} N M g \equiv \left(\frac{\mathcal{L}}{\xi} \right)^2 \quad (11)$$

$$w_L = \frac{1}{L^2} \frac{N\alpha}{\omega_0/K} = \frac{1}{\mathcal{L}^2} \frac{N\alpha}{m\omega_0} \equiv \left(\frac{\mathcal{R}}{\lambda} \right)^2 \quad (12)$$

Later we discuss their significance, and clarify that u_L and w_L are the *classical* dimensionless parameters that control the emergence of SF and SC respectively.

In the quantum treatment we have to specify also N . Note again that in the so-called second quantization scheme $1/N$ plays the role of a dimensionless Planck constant. As explained in [\[18\]](#) (and references therein) the

Mott transition is controlled by the *quantum* dimensionless parameter

$$\gamma_L = \frac{u_L}{N^2} \quad (13)$$

In the continuum GPE limit this parameter controls the crossover to the hard-core bosons regime where the particles can be regarded formally as fermions.

The Hamiltonian [Eq. \(7\)](#) is a closely related to the familiar model of coupled Josephson junctions. Assuming equal site occupation ($n_j := N/L$), it is like the SQUID Hamiltonian of [Appendix B](#) with $E_C = U$ and $E_J = NK/L$. Thus we make the identification $\gamma_L = E_C/E_J$, and point out that u would become meaningless (for example, there is no meaning to discuss $u=0$ condensation in momentum orbitals).

The parameter ξ that is defined via [Eq.\(11\)](#) is the standard definition of the healing length in the GPE context. The parameter λ that is defined via [Eq.\(12\)](#) is motivated by the discussion of the London penetration depth in [Appendix C](#). For a thin ring it is merely a formal notation, and the ratio $\kappa = \lambda/\xi$ has no practical meaning.

IV. SUPERFLOW

The essence of superfluidity (SF) and superconductivity (SC) is the feasibility of superflow. This superflow is a metastable condensation of the particles in an excited momentum orbital. As opposed to that, we have eigenstates with fragmented (FR) occupation that possibly support microscopic rather than macroscopic persistent current. In this section we summarize the “big picture” regarding the emergence of superflow and its dependence on the major dimensionless parameter of the model. In the subsequent sections we provide a more detailed account.

A. Superfluidity (SF)

If $\alpha = 0$, the variable ϕ becomes constant of motion, and the Hamiltonian of the ring becomes formally identical to that of an SF circuit in a rotating frame, where ϕ is the Sagnac phase (proportional to the rotation velocity). Depending on the strength of the interaction, such ring can support superflow: a metastable persistent current due to condensation of particles in an excited momentum orbital.

In the absence of interaction ($u = 0$), the ground-state of a non-rotating ring ($\phi = 0$) is the condensation in the $k_0 = 0$ orbital. As we turn on the interaction (keeping $\phi = 0$), additional condensates at k_m may become metastable. We refer to this as SF. To be precise, due to the interaction the ground-state and the metastable states become *squeezed* coherent states, meaning that the occupation of the k_m orbital exhibits some depletion. Unlike the $m = 0$ ground-state, the $m \neq 0$ metastable

states are immersed in quasi-continuum of FR states that are possibly supported by chaotic regions in phase-space [\[18\]](#). Quantum mechanically their meta-stability is endangered by tunneling.

An equivalent way to describe the meta-stability is to say that the k_0 condensate remains metastable in a rotating frame, namely, within a range $|\phi| < \phi_c$, where ϕ_c is the (dimensionless) critical velocity that is implied by the Landau criterion, which we further discuss below in subsection C of [Sec. \(V\)](#).

B. Superconductivity (SC)

The other way to gain metastability (not related to U) is encountered once ϕ becomes a dynamical coordinate. We refer to this as SC. This coordinate can adjust itself such that the k_m condensate becomes meta-stable. The idea is easily understood if one assumes $u = 0$. Then the occupations of the orbitals become constant of motion. Dropping a constant, we get for a given occupation $\mathbf{n}_k \mapsto n_k$ the following Hamiltonian

$$\mathcal{H}_{osc} = \frac{\omega_0}{2} \left[\frac{\alpha}{2} \mathbf{n}_{osc}^2 + \frac{2}{\alpha} \phi^2 \right] - N_s K \cos \left(\frac{\phi}{L} - \bar{k} \right) \quad (14)$$

In the above expression the definitions of N_s and \bar{k} are implied via [Eq.\(8\)](#). For condensation in the k_m orbital we get $\bar{k} = k_m$, and $N_s = N$ attains its maximal value. If α is large enough, ϕ can adjust to a value $\phi \sim \phi_m$, where

$$\phi_m = 2\pi m, \quad [m = \text{integer}] \quad (15)$$

such that the condensate becomes metastable. The energetic price for that is $E \sim (\omega_0/\alpha)\phi_m^2$. Due to this symmetry breaking we get an SC-type superflow. Irrespective of that, most eigenstates feature fragmented (FR) occupation for which the effective N_s is smaller compared with N .

For non-zero interaction u [Eq. \(14\)](#) can be regarded as an effective approximation. The condensates are no longer exact eigenstates. Due to the squeezing they exhibits some depletion, which implies that they do not feature maximal N_s . For very large u the ground state becomes MI, with equal occupation of the orbitals, for which $N_s = 0$.

V. THE ENERGY LANDSCAPE

The energy landscape is dictated by 3 relevant energy scales

$$W_K = \frac{NK}{L^2} \quad (16)$$

$$W_U = \frac{N^2 U}{L} \quad (17)$$

$$W_\Phi = \frac{\omega_0}{\alpha} \quad (18)$$

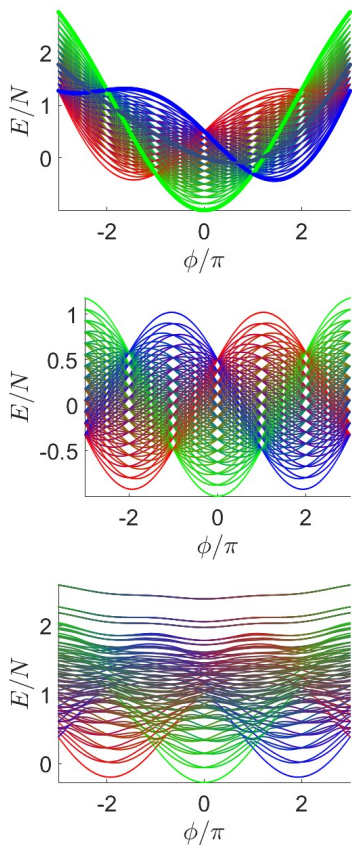


FIG. 1. **Born-Oppenheimer energies.** The 91 energy levels of an $N = 12$ trimer as function of ϕ . From up to down, the model parameters are $u = 0, 0.5$ and $\alpha = 2, 20, 20$, while $\omega_0 = 0.48$. The units of time here and in subsequent figures are chosen such that $K = 1$. We use RGB color-code for the occupation as explained in the text. Most of the levels cannot be resolved, and therefore in the left panel we highlight representative energy levels: full condensation in the k_0 orbital (green); full condensation in the k_+ orbital (blue); and fragmented 20% 30% 50% occupation (grayish).

Note that division of the W -s by N are the “classical” parameters Eq.(10) of the model. Their significance is as follows: Up to numerical prefactor, W_K is the price of having a condensation in the next excited orbital $k_1 = 2\pi/L$. Looking on the 3rd term of Eq.(8) one realizes that due to the interaction a condensate has lower energy compared with a fragmented state, where the price of fragmentation is W_U . Finally, in the SC context, W_Φ reflects the price of non-zero flux $\phi_1 = 2\pi$. The associated dimensionless parameters u_L and w_L of Eq.(11) and Eq.(12) are the ratios W_U/W_K and W_K/W_Φ respectively. If u_L is too large, the condensate get fragmented, aka Mott transition, and the superflow is diminished. The dimensionless parameter that controls this transition is γ_L of Eq.(13). Note that in the SF context finite u is essential to create the metastability, but if u is too large, it diminishes this metastability. As opposed to that, u is not required for getting the SC metastability.

A. Potential floor

In order to figure out what are the metastable flow states of the system, it is convenient to regard $|\phi, n_k\rangle$ as the configuration space. Then one can define the potential floor as

$$V(\phi, n_k) = \min[\mathcal{H}] \quad (19)$$

where the minimum is taken with respect to the conjugate coordinates. Note that at this stage of the analysis we adopt a semiclassical perspective and ignore quantum uncertainties.

In order to get visualization of the energy landscape let us first neglect in Eq.(8) the interaction induced transitions, meaning that the occupations n_k of the orbitals become good quantum numbers. Each $\{n_k\}$ configuration defines via Eq.(14) a potential-energy that can be regarded as the *Born-Oppenheimer* level with regard to the ϕ coordinate. We refer to them below as *washboard-sections*. The major washboard-sections correspond to k_m condensates defined as $n_k = N\delta_{k,k_m}$. The intermediate washboard-sections correspond to fragmented occupation.

B. Valley structure

The potential floor feature a *valley structure*. There is a major valley around the k_0 condensate at ϕ_0 , and possibly there are several metastable valleys around the k_m condensates at $\phi \sim \phi_m$. An illustration is given in Fig.1a where the lowest valley is indicated by a green color, and the two metastable valleys are indicated by red and blue colors. The energies of the meta-stable minima are $E \sim W_\Phi m^2$, and they are separated by barriers whose height is of order W_K . Accordingly, the energy floor features $\sim w_L$ major valleys. For large enough α there are L major valleys, each correspond to a different condensate. They are located at the smallest values of ϕ_m . Due to the discreteness of the ring there might be also secondary valleys, for larger $|m|$ values.

In the absence of interaction each whasboard-section holds eigenstates that can be labeled by the occupations n_k and by a running index $\nu_{osc} = 0, 1, \dots$. Those unperturbed eigenstates can be categorized into two groups: those that reside inside the valleys, and those that reside “above” the energy barriers. As the interaction is switched on, states of different washboard-sections are mixed, unless they reside inside valleys that are separated by an energy-barrier.

C. Landau Grooves

The major washboard-sections that correspond to k_m condensates are separated by intermediate washboard-sections that correspond to fragmented occupation. The

3rd term of Eq.(8) implies that due to an energy cost W_U , a condensates might have lower energy compared with fragmented states of the nearby washboard-sections. To be more precise, the valley that is associated with the k_m condensate looks like a *groove* that is formed in the potential floor $V(n_k, \phi)$. This groove is centered at ϕ_m , and its stretch along the ϕ direction is determined by the Landau criterion as explained below.

Holding ϕ fixed is formally like considering a rotating ring. A condensate, say at k_0 , is a local minimum of the potential if all the Bogolyubov frequencies are real and positive. The lowest excitation frequency ω_q is given by Eq(B2) of [25]) with $q = \pm 2\pi/L$. If the ring is large ($L \gg 1$) an approximation is $\omega_q \approx c|q| \pm v_\phi q$, where $c = (K/L)\sqrt{u_L}$ is the speed of sound and $v_\phi \approx (K/L)\phi$ is the rotation velocity of the ring. Hence we get the Landau criterion for stability $|\phi| < \phi_c$, where $\phi_c = \sqrt{u_L}$. More generally, if L is not large, it is straightforward to deduce that critical value is determined by

$$2 \cos\left(\frac{\phi_c}{L}\right) = -\left(\frac{u_L}{L^2}\right) + \sqrt{\left(\frac{u_L}{L^2}\right)^2 + 4 \cos^2\left(\frac{q}{2}\right)} \quad (20)$$

Consistency with the large L approximation is easily verified. Optionally, given L , the critical value ϕ_c increases with u_L from the minimal value $\phi_c \sim \pi$ to the limiting value $\phi_c \sim (L/2)\pi$.

More generally, the conclusion is that a condensate $n_k = N\delta_{k,k_m}$ of a rotating ring is energetically stable if $|\phi - \phi_m| < \phi_c$. This means that the potential floor $V(\phi, n_k)$ features parallel *grooves* in the ϕ direction. It follows that the number of flow-states for a given ϕ equals $\sim \phi_c/\pi$, and increases with u_L from 1 to $L/2$.

D. Meissner Grooves

In addition to the short-range interaction U there is also a long-range electrostatic interaction \mathcal{U}_{EM} . We shall discuss the implication of this interaction, on equal footing with the U interaction, in Sec. (X). The bottom line, based on Bogoliubov analysis of the low excitations, is that the Grooves are further deepened and in some sense an excitation gap can form.

Concluding this section: *the interaction has two opposing effects*. On the one hand it creates Grooves that can support meta-stable condensates for fixed ϕ , which is the explanation of Landau for the feasibility of super-flow. On the other hand, it couples the different washboard-sections, leading to ergodization, and hence worsening the conditions for meta-stability. Eventually, for large enough interaction, superflow is diminished due to the formation of Mott insulator.

VI. THE SF-SC BORDER

For small α , the only metastable states that can exist are SF-type as implied by the Landau stability condition.

But as α is increased, the question arises whether there are *additional* valleys at $\phi_m \neq 0$ that can support SC-type metastable states. We refer to this as the SF-SC transition. The existence of SC-type metastable states depends on the model parameters, notably on α and u , as discussed here and in subsequent sections.

For weak interaction the condition for having a barrier between the k_0 condensate and the k_1 condensate can be worked out as follows: Define $E = f_k(\phi)$ as the energy Eq.(14) for a condensation in orbital $k = 0, \pm$ given ϕ . In Fig.1 the green curve $f_0(\phi)$ and the blue curve $f_+(\phi)$ frame two Born-Oppenheimer washboard-sections that intersect at $\phi = \pi$. This is where we can have a barrier between the two valleys that accommodate condensates. The condition for having this barrier is $f'_+(\phi = \pi) < 0$, leading to the identification of the SC regime:

$$2\pi \frac{\omega_0}{\alpha} < \frac{1}{L} \sin\left(\frac{\pi}{L}\right) NK \quad (21)$$

Note that the two sides correspond to W_Φ and W_K respectively. The ratio between them corresponds to the dimensional parameter w_L whose significance has been discussed in Sec. (V).

If non-zero interaction U is introduced, the transitions that were neglected in Eq.(8), lead to some depletion, say of $\sim n_{dep}$ particles, and consequently the effective value of N in Eq. (21) becomes smaller. For uniformly distributed depletion we get $N_s = N - [L/(L-1)]n_{dep}$. In the extreme case, for equal occupation of the orbitals, as in the MI regime, we get $N_s = 0$. The implication is that for strong interaction (large U) the meta-stability diminishes.

VII. CHARACTERIZATION OF EIGENSTATES

In the previous sections we have discussed the topography of the energy floor, and the implication on the existence of metastable flow-states. But we would like to adopt a more comprehensive perspective that allows identification of regions in the spectrum, semiclassical-related classification of the eigenstates, and detection of fingerprints of underlying chaos. For this purpose we define several useful measures.

Given $(N, N_{osc}, K, U, \omega_0, \alpha)$ we diagonalize the Hamiltonian Eq.(7), get the eigen-energies E_ν and the eigen-functions $\Psi_{n_{ring}, n_{osc}}^{(\nu)}$. Here the index $n_{ring} \equiv \{n_k\}$ indicates the Fock orbital-occupation basis states, and n_{osc} indicates the occupation basis states of the EM mode. For a trimer ring the dimensionality of Hilbert space is $\mathcal{N} = \mathcal{N}_{trimer}\mathcal{N}_{osc}$, where $\mathcal{N}_{trimer} = (1/2)(N+1)(N+2)$ and $\mathcal{N}_{osc} = (N_{osc}+1)$.

A. Occupation measures

For each eigenstate we calculate the the orbital occupations $\langle n_k \rangle$. For the trimer we label the three orbitals as

$k = 0, \pm$. In the figure we use RGB color-code as follows:

$$RGB = \left(\frac{\langle \mathbf{n}_- \rangle}{N}, \frac{\langle \mathbf{n}_0 \rangle}{N}, \frac{\langle \mathbf{n}_+ \rangle}{N} \right) \quad (22)$$

If we focus on the EM mode, then complementary information is provided by $\langle \phi \rangle$ and $\langle \mathbf{n}_{osc} \rangle$.

B. Condensation measures

The one-body reduced probability matrix of particles in the ring, and the reduced probability matrix of the oscillator, are

$$\rho_{k,k'}^{(ring)} = \frac{1}{N} \langle a_k^\dagger a_{k'} \rangle \quad (23)$$

$$\rho_{n,n'}^{(osc)} = \sum_{n_{ring}} \Psi_{n_{ring},n} \Psi_{n_{ring},n'}^* \quad (24)$$

There is no disorder in our Hamiltonian, and therefore $\rho_{k,k'}^{(ring)}$ is diagonal. Consequently, we define condensation and entanglement measures:

$$\mathcal{S}_{purity} = \text{trace}([\rho^{(ring)}]^2) = \sum_n \left[\frac{\langle \mathbf{n}_k \rangle}{N} \right]^2 \quad (25)$$

$$\mathcal{S}_{ent} = \text{trace}([\rho^{(osc)}]^2) \quad (26)$$

Roughly, $1/\mathcal{S}_{purity}$ is the number of participating orbitals, such that $\mathcal{S}_{purity} = 1$ implies condensation in a single orbital. Irrespective of that $\mathcal{S}_{ent} = 1$ implies that the ring-osc eigenstate can be factorized, which is the case for either full SF condensation or strict MI fragmentation. We define $\mathcal{N}_{ent} = 1/\mathcal{S}_{ent}$, and note that $\log[\mathcal{N}_{ent}]$ is like entanglement entropy.

C. Ergodicity measures

The participation number \mathcal{M} tells us how many basis Fock states participate in the formation of an eigenstate. Considering either site or orbital basis we extract the probabilities $p_{n_{ring}} = \sum_{n_{osc}} |\Psi_{n_{ring},n_{osc}}|^2$. Then we calculate the participation number

$$\mathcal{M} = \left[\sum_n p_n^2 \right]^{-1} \quad (27)$$

See e.g. [18], and note that this is equivalent to the calculation of generalized fractal dimension as in e.g. [16, 17]. An individual eigenstate is possibly not ergodic, and does not fully accommodate the energetically allowed space. In order to determine the volume of the allowed space, we calculate the averaged p_n within the energy window of interest, and then calculate the associated participation number which we denote as $\bar{\mathcal{M}}$. The ratio $\mathcal{M}/\bar{\mathcal{M}}$ serves

as a quantum ergodicity measure. For a fully chaotic system such as billiard one expects it to be somewhat less than unity due to fluctuations. In practice the value is much smaller indicating lack of ergodicity. We calculate both \mathcal{M}_{sites} in the site basis, and $\mathcal{M}_{orbitals}$ in the orbital (momentum) basis, and plot

$$\mathcal{M} \equiv \min [\mathcal{M}_{sites}, \mathcal{M}_{orbitals}] \quad (28)$$

Few words are in order regarding the reasoning behind this definition. Let us discuss a general (abstract) system with basis states $|n\rangle$. Consider an eigenstate $|E\rangle$ and associated probability matrix $\rho_{n,m} = \langle n|E\rangle \langle E|m\rangle$. More generally consider $\rho_{n,m}$ that is obtained by averaging over a small energy window. Clearly $\text{Tr}[\rho^2]$ reflects the number of eigenstates that have been mixed. Furthermore, we have the inequality $\text{Tr}[\rho^2] > \sum_n p_n^2 \equiv \mathcal{S}_{basis}$, where $p_n = \rho_{n,n}$. Formally we can say that $\text{Tr}[\rho^2]$ is the maximum \mathcal{S}_{basis} over all possible bases. Or equivalently we say that \mathcal{M} is the minimum participation over all bases. If we restrict the minimization over semiclassically-meaningful bases, we get an operative definition for the volume of the *energy shell*. If the individual eigenstates are say localized, then the semiclassical volume $\bar{\mathcal{M}}$ of the energy shell becomes relatively large, with negligible dependence on the energy-width of the averaging window, see e.g. demonstration in [27]. Accordingly the ratio $\mathcal{M}/\bar{\mathcal{M}}$ provides a practical estimate for the fraction of the energy-shell that is occupied by an individual eigenstate.

VIII. TOMOGRAPHY OF THE SPECTRUM

We demonstrate numerically spectrum tomography for the simplest circuit, namely, a trimer ring ($L=3$). Depending on parameters such ring can support either an SF ground-state or SC multi-stability. In practice α of Eq. (6) is very small, but the SF-SC transition is feasible because $N\alpha$ can be large. In the numerics N is limited, and therefore we artificially compensate it by setting unrealistic large α . Nevertheless, the outcome is semiclassically equivalent, and therefore satisfactory for the purpose of illustration.

Note that the Landau criterion implies that SF meta-stability (as opposed to SC meta-stability) requires more than four sites ($L > 4$). With 3 sites, SF meta-stability can be demonstrated if the ring is rotating (with $\phi \sim \pi$), see Appendix H of [18], which in the present context would be equivalent to the introduction of an external flux Φ_{ext} as explained in Appendix B.

A. Spectra

Fig. 2 displays images for selected eigenstates of an $L = 3$ circuit for $U = 0$. Namely, each row is an image of the ϕ probability distribution for an eigenstate

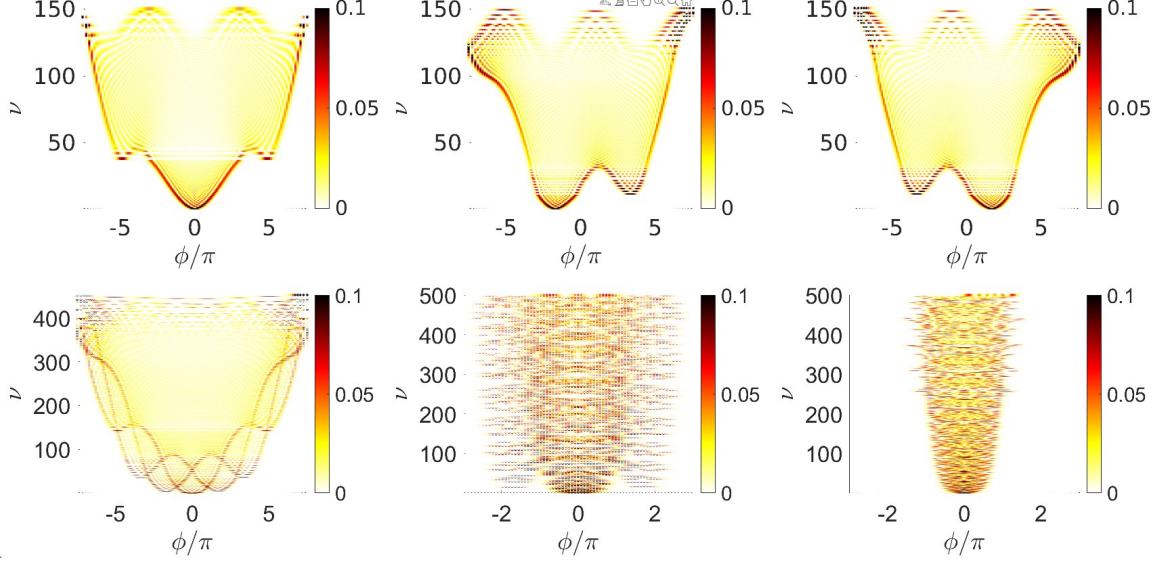


FIG. 2. **The energy landscape:** We consider $u=0$ trimer with $N = 12$ particles coupled to an EM mode. The other parameters are $\omega_0 = 0.48$ and $\alpha = 2$, while $N_{osc} = 150$. The upper panels provide images for eigenstates of \mathcal{H}_{osc} Eq.(14) assuming that the particles are condensed in one of the three k orbitals. Each row is the ϕ probability distribution. The rows are ordered by energy. The lower left panel combines the 3 upper upper panels. It would be the full spectrum if we had a single particle. For $N = 12$ one has to combine the spectra that are associated with all possible occupations. The outcome (zoomed) is the middle lower panel. In the right lower panel we display the result for $\alpha = 1/2$, where SC multi-stability is absent.

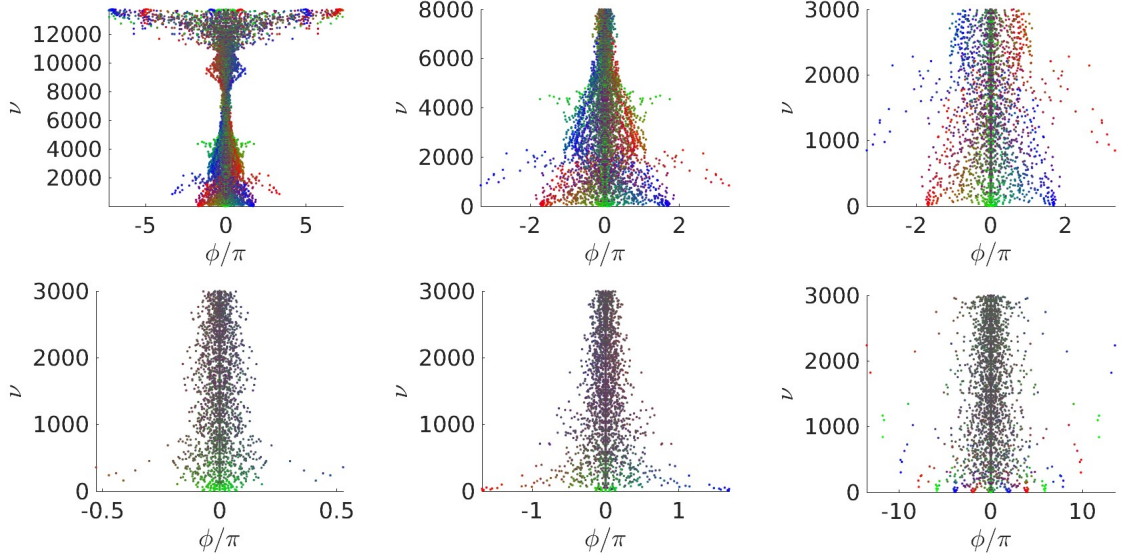


FIG. 3. **Tomography of the spectrum:** The spectrum for trimer with $N = 12$ particles, coupled to an EM mode with $\omega_0 = 0.48$ and $N_{osc} = 150$. Each eigenstate is represented by a point that is positioned according to its energy index ν and its $\langle \phi \rangle$. The RGB color-code indicates the occupation of the orbitals. In the first row the interaction is $u = 1/2$ and the coupling is $\alpha = 2$. The two right panels are zoomed versions of the left panel, where the upper false eigenstates that appear due to finite N_{osc} are truncated, and the SC multi-stability is highlighted. In the second row the interaction is $u = 3$ and the couplings, from left to right, are $\alpha = 1/2, 2, 20$. The panels are zoomed over the first 3000 states. This set demonstrates the crossover from SF to SC multi-stability. Note that the range of the horizontal axis has been adjusted.

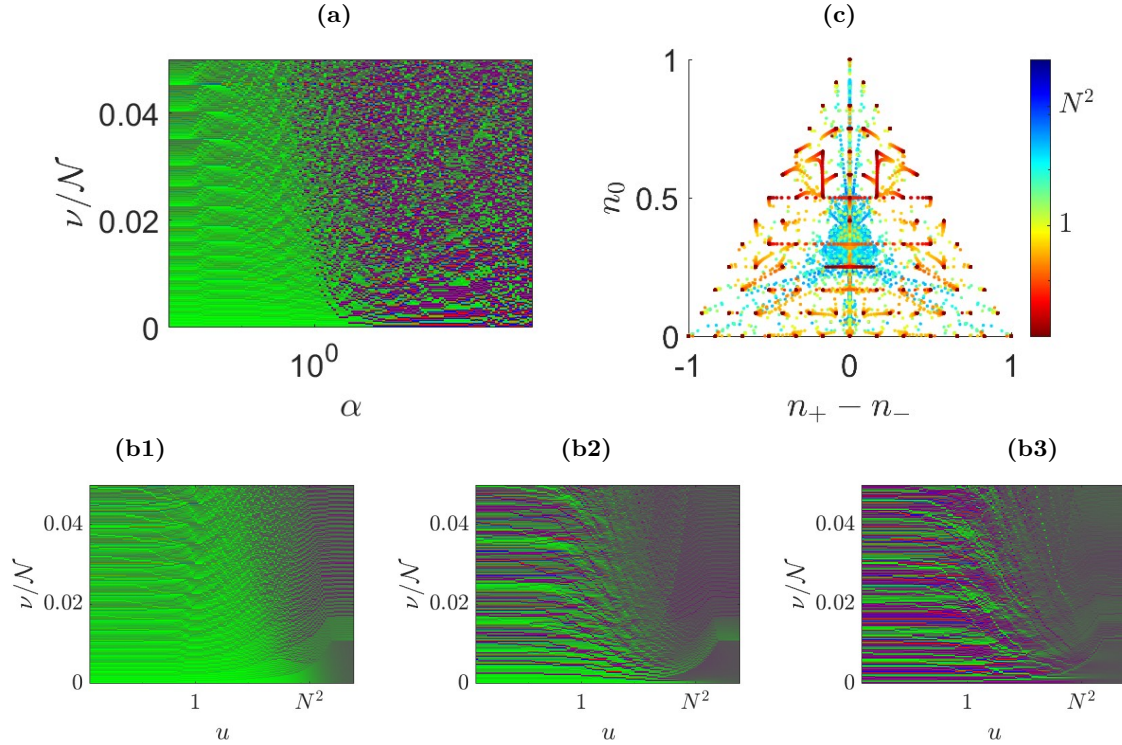


FIG. 4. **The formation of SC multi-stability:** (a) Each column is an image of the spectrum for a different value of α . The energy levels (indexed by ν) are RGB color-coded, reflecting orbital occupation as explained in the text. The interaction between the particles is weak ($u = 0.01$). The other parameters are $\omega_0 = 0.48$, and $N = 12$ and $N_{osc} = 60$. The states are in the range $0 < \nu < 0.05\mathcal{N}$, namely, the 277 lowest levels out of 5551 are displayed. (b) The dependence of the spectrum on u for representative values of EM coupling, namely, $\alpha = 0.1, 1, 20$. This set demonstrates the crossover from SF to SC, and how SF/SC is diminished due to u . (c) The information of panel b3 is displayed in a different way. Each point is positioned according to the normalized orbital occupations, and the color-code indicates u . As the interaction is increased multi-stability is diminished.

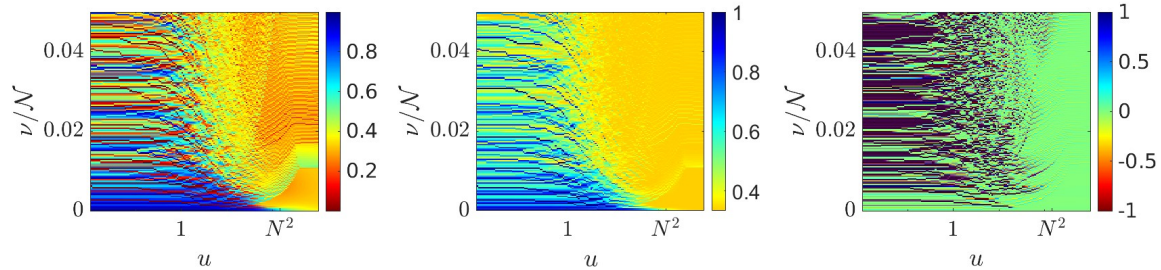


FIG. 5. **Multi-stability versus interaction.** Optional diagrams that show the u dependence of the spectrum. The 3 panels are: (a) The normalized occupation n_0 of the zero momentum orbital; (b) The purity S_{purity} serves as a condensation measure; (c) The EM mode flux $\langle \phi \rangle$ serves to identify SC symmetry breaking. The parameters are $N = 12$, and $N_{osc} = 60$, and $\alpha = 2$, and $\omega_0 = 0.48$.

of Eq.(14). The zoomed panels show images of all the low-lying eigenstates for $\alpha = 1/2$ and $\alpha = 2$. The latter exhibits SC multi-stability as opposed to the former that feature an SF ground-state. A numerical remark is in order here. Mathematically speaking quasi-degenerated SC metastable states should combine into cat-state superpositions that feature $\langle \phi \rangle = 0$, but we care to introduce a numerically negligible bias Φ_{ext} that allows ‘spontaneous’ breaking of this symmetry.

Fig.3 displays the full spectrum for non-zero interaction. Each eigenstate is represented by a single point that is RGB color-coded such that red, green, and blue indicate the respective occupations (n_-, n_0, n_+) . The n_k are not ‘good quantum numbers’ but rather are expectation values. The selected set of panels clearly demonstrates the crossover from SF to SC multi-stability.

B. Regimes

We construct regime diagrams to show the dependence of the spectrum on the coupling α and on the interaction u . In Fig.4 each column is an RGB color-coded spectrum. Fig.4a is an (α, E) regime diagram. Green region indicates SF states for which $\langle \phi \rangle = 0$, while scrambled

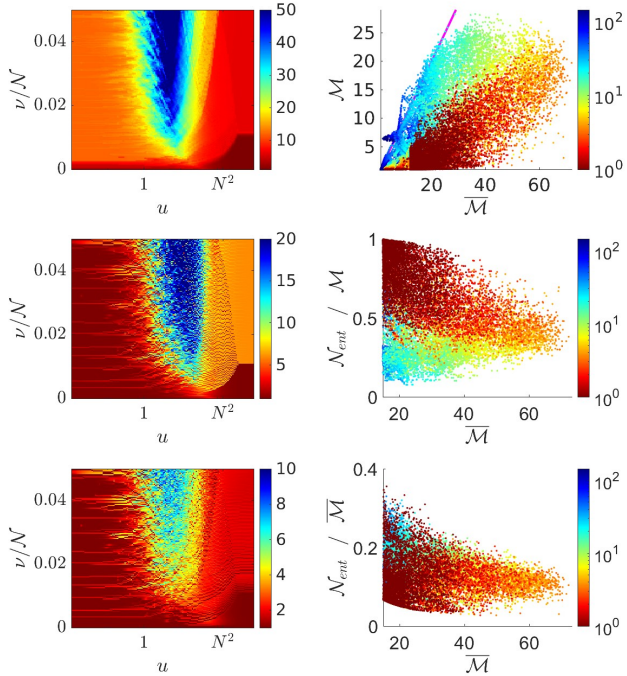


FIG. 6. **Ergodicity and Entanglement:** Left panels from top to bottom: images of $\bar{\mathcal{M}}$ and \mathcal{M} and \mathcal{N}_{ent} . The parameters are the same as in Fig.5. Right panels: scatter diagrams color-coded by u , for inspecting correlations between the 3 measures. The upper diagram allows to characterize the degree of ergodicity. For reference we plot a diagonal magenta line that indicates full ergodicity. The two other diagrams demonstrate that \mathcal{N}_{ent} is more correlated with $\bar{\mathcal{M}}$ than with \mathcal{M} .

RGB region indicates SC multi-stability associated with broken symmetry $\langle \phi \rangle \neq 0$. The observed SF-SC transition roughly agrees with the border of Eq.(21), and will be further discussed in Sec. (IX).

Fig.4b demonstrates how the multi-stability is diminished as u is increased. This is the transition to the MI regime where the eigenstates get fragmented in the Fock site basis. Optional visualizations of this dependence is provided in Fig.5 where we inspect separately the occupation n_0 of the zero momentum orbital; the purity S_{purity} that serves as a condensation measure; and $\langle \phi \rangle$ that serves to identify the SC symmetry breaking.

C. Ergodicity

The underlying phase space is in general chaotic and possibly mixed with quasi-regular motion. In order to diagnose this aspect we provide in Fig.6 the (u, E) diagrams for both $\bar{\mathcal{M}}$ and \mathcal{M} . Then we construct a scatter diagram to characterize the degree of ergodicity. We see that accessible phase space region expands at the transition, indicated by $\bar{\mathcal{M}}$. Crossing the diagram in the increasing u direction, the ergodicity increases slowly as indicated by the ratio $\mathcal{M}/\bar{\mathcal{M}}$.

D. Entanglement

We provide in Fig.6 the (u, E) diagrams for the entanglement measure \mathcal{N}_{ent} . The associated scatter diagrams show that it is correlated with $\bar{\mathcal{M}}$ and not much with \mathcal{M} . In other words, the entanglement reflects the geometry of the accessible energy surface and not its chaoticity. Irrespective of that \mathcal{N}_{ent} is bounded by \mathcal{M} , which is responsible to a residual breakdown of the correlation in the small u region.

To explain the correlation with $\bar{\mathcal{M}}$, we point out that by definition \mathcal{N}_{ent} is a measure for the influence of n_{osc} on the accessible phase-space region of the ring. Maximum entanglement is achieved if the relative regions are ‘orthogonal’. Whether the motion in a given accessible region is ergodic or not, does not affect much the overlap between the relative regions.

E. Borders

The dependence of the spectrum on ω_0 is shown in Fig.7, featuring SC/SF/FR regions. It is further discussed in the next section.

Placing the focus only on the low-lying levels, one can construct an SF-SC-MI diagram as demonstrated in Fig.8. This diagram highlights the α -related SF-SC border of Eq.(21), and the u -related MI transition that is further discussed in the next section. In order to identify numerically the 3 regimes we have improvised an

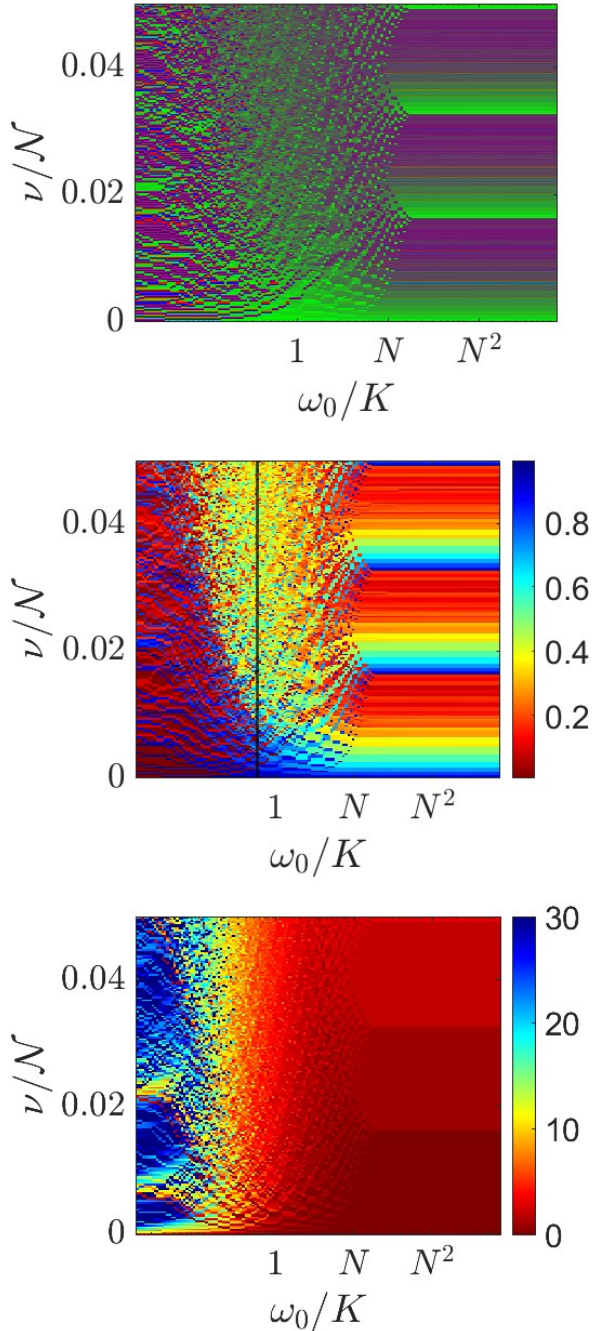


FIG. 7. **Multi-stability versus mode frequency.** The diagrams show the dependence of the color-coded spectrum on the mode frequency ω_0 . The 3 panels from top to bottom are: (a) RGB-coded occupation; (b) The normalized occupation n_0 of the zero momentum orbital; (c) The occupation n_{osc} of the cavity mode. The other parameters are $\alpha = 2$ and $u = 3$, while $N = 12$ and $N_{osc} = 60$. As ω_0 is increased the low states go through an SC region (where we have multi-stability); and an SF regime (where we have single-stability). Above the SC/SF region we have a fragmented regime (FR). To the right of the SC/SF/FR regimes we have an n_0 rainbow region where $n_{osc} = 0, 1, 2$.

ad-hoc measure that is based on \mathcal{S}_{purity} and on the zero-momentum orbital occupation n_0 .

IX. THE SC/SF/FR SPECTRAL REGIONS

The tomography allows the identification of SC/SF/FR/MI regions in the full quantum spectrum. As model parameters are varied, it is not just the ground state that is affected. We already identified in previous section the MI region using (u, E) diagrams. We now focus on the identification of the SC/SF/FR regions, keeping away from the MI region (i.e. we assume small u). The most illuminating figure is possibly Fig. 7b with complementary panels (a, c). In order to understand the illustrated dependence of the spectrum on ω_0 we have to clearly distinguish between classical and quantum borders. The classical borders are determined by the classically-scaled parameters $(NU/K, \omega_0/K, N\alpha)$, whereas quantum borders involve extra N dependence ($1/N$ plays the role of Planck constant). For example the MI border is $u_L \sim N^2$

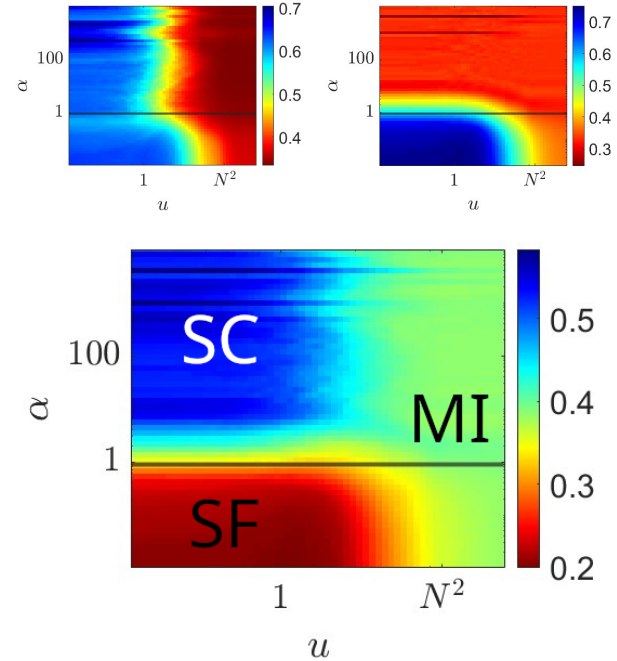


FIG. 8. **SF-SC-MI regime diagram.** The transitions between these regimes is detected by looking on the dependence of averaged measures on model parameter (u, α) . Other parameters are $N = 12$ and $N_{osc} = 60$ and $\omega_0 = 0.48$. The average is over the eigenstates in the energy range $0 < \nu < 0.05N$. The 3 panels are: (Left-) The measure \mathcal{S}_{purity} indicates condensation; (Right-) The measure $\overline{(n_0/N)}$ indicates zero orbital condensation; (Bottom-) An ad-hoc combination of the previous panels, namely, $[1 - \overline{(n_0/N)}](\mathcal{S}_{purity})^{1/2}$, effectively provides the desired regime diagram. The horizontal black line is the expected SF-SC metastability border.

for the ground state and $u_L \sim N$ for excited states as discussed in [18].

The semiclassical analysis of meta-stability has implicitly assumed that the topography of the energy floor, and in particular of the Landau grooves, can be resolved quantum mechanically. The quantum borders are implied by inspection of the conditions for that. From the perspective of Eq.(14), the question is whether or how many eigenstates can be accommodated by a given valley.

As a preliminary stage let us discuss the quantum significance of α . If $\alpha < 1$ there is a sequence of $\sim 1/\alpha$ lowest states that have energy spacing $\sim \omega_0$, and are contained in the k_0 groove. The next states belong to the k_1 groove whose energy floor is higher, namely $W_\Phi = \omega_0/\alpha$. From now on let us assume for simplicity that $\alpha > 1$, meaning that subsequent states belong to different grooves. Let us call it “scrambled SC region” of the spectrum.

The next question that arises is how many eigenstates can be accommodated by each groove. The rough estimate is determined by the inequality

$$\nu < \frac{W_K}{\omega_0} \quad (29)$$

This determines the scrambled SC region in Fig.7b. This region features mix of blue and red eigenstates, indicating multi-stability. The $1/\omega_0$ dependence of its border is apparent. As ω_0 is further increased the classical SC-SF border is crossed, and then only the blue eigenstates remain. Above the SC/SF region we see yellowish eigenstates, indicating the FR region.

The right-most quantum region that we see in Fig.7b is $\omega_0 > NK$. This condition implies that the eigenstates do not resolve the topography of the potential floor. The orbitals form an energy band of width $2K$, and therefore all the possible manybody excitations of the ring are in the range whose width is $2NK$. Consequently, the spectrum *separates* into sequences of states that have the same ν_{osc} , as confirmed by Fig.7c.

X. MEISSNER EFFECT

The Meissner effect in the simplest way is explained as a screening effect due to the coupling of the ring to the EM mode. See Appendix B for a concise summary that clarifies that the dimensionless screening parameter is w_L of Eq.(12). An optional way to express this dimensionless parameter is $w_L = (\omega_p/\omega_0)^2$, where the effective plasma frequency is

$$\omega_p^2 = \alpha \omega_0 \frac{NK}{L^2} \sim \frac{e^2}{M} \left(\frac{N}{\mathcal{R}^3} \right) \quad (30)$$

In a more careful treatment, as presented below, we have to distinguish between ω_p that involves the total number N of particles, and ω_s that involves the effective number N_s of superfluid carriers.

The Meissner effect can be regarded as a Higgs mechanism that provides mass to the EM mode. In a field-theory perspective the bare EM model have very small frequency ω_0 that goes to zero for large cavity (small wavelengths), meaning that the EM field is massless. Due to the coupling to the condensate the EM field acquires a mass (hence the London penetration distance). This mass (frequency) is proportional to the *condensate density*. Here we have a mesoscopic version of the Higgs mechanism. Namely, the bare frequency ω_0 is increased. In the Harmonic approximation, based on Eq.(8), it becomes

$$\omega = \sqrt{\omega_0^2 + \omega_s^2} \quad (31)$$

where ω_s^2 is defined as $(1/2)\omega_p^2$ of Eq.(30) with N replaced by N_s .

Acquiring extra mass is not the whole story of the Anderson-Higgs mechanism [7–10]. For bulk superconductor, the associated statement is that the Goldstone excitations become gapped and can be regarded as an extra longitudinal mode of the EM field. This statement requires further clarification and adaptation in the mesoscopic context. The gap is actually created due to the electrostatic interaction \mathcal{U}_{ES} of Eq.(A4). Namely, any long wavelength modulation of the charge-density has a large energy cost $\sim \omega_p$.

Let us see how the electrostatic interaction looks like for our Bose-Hubbard ring. We can express \mathcal{U}_{ES} as a function of the site occupation operators. For this purpose we define

$$\delta n_j = \mathbf{a}_j^\dagger \mathbf{a}_j - \frac{N}{L} = \frac{1}{L} \sum_{k' \neq k} a_{k'}^\dagger a_k e^{-i\varphi r_j} \quad (32)$$

where $a_{k'}^\dagger a_k$ destroys particle in orbital k and creates it in orbital k' , while $\varphi = k' - k$ is the associated change in the momentum. The position of the site along the chain is r_j modulo \mathcal{L} , while its actual position in space will be denoted as \mathbf{r}_j . We use here units of length such that the distance between sites is unity. The electrostatic energy is

$$\mathcal{U}_{ES} = \frac{1}{2} \sum_{i,j} \delta n_i \delta n_j \frac{e^2}{|\mathbf{r}_i - \mathbf{r}_j|} \quad (33)$$

$$= \frac{e^2}{L} \sum_{\varphi} f(\varphi) \left[a_k^\dagger a_{k+\varphi} a_{k+\varphi}^\dagger a_k + a_{k-\varphi}^\dagger a_k a_{k+\varphi}^\dagger a_k \right] \quad (34)$$

where

$$f(\varphi) = \frac{1}{2} \sum_{r \neq 0} \frac{\cos(\varphi r)}{|r|} \quad (35)$$

For bulk superconductor $f(\varphi) \sim 1/\varphi^2$ but for our one-dimensional chain $f(\varphi) \sim \ln(1/\varphi)$. Assuming that most of the particles are condensed in the $k=0$ orbital, we

can use the usual Bogoliubov approximation for the interaction-induced transitions between orbitals:

$$\sum_{\mathbf{q}} \Delta_{\mathbf{q}} \left[a_{-\mathbf{q}}^\dagger a_{\mathbf{q}}^\dagger + a_{\mathbf{q}} a_{-\mathbf{q}} \right] \quad (36)$$

where

$$\Delta_{\mathbf{q}} = \frac{N}{L^2} \left[\frac{e^2}{\ell} \right] f(\mathbf{q}) \quad (37)$$

Here we restored in the square brackets general physical units by introducing the lattice constant ℓ .

The ring Hamiltonian contains the kinetic term $\sum_k (\varepsilon_k + \Delta_k) n_k$, based on the second term of Eq.(8) and the first term of Eq.(34). Consequently, following the standard textbook derivation, the low lying Bogoliubov frequencies are

$$\omega_{\mathbf{q}} = \sqrt{\left[\varepsilon_{\mathbf{q}} + 2 \left(\frac{NU}{L} + \Delta_{\mathbf{q}} \right) \right] \varepsilon_{\mathbf{q}}} \quad (38)$$

where the NU/L term originates from the last term of Eq.(8). The bottom line is that the usual BH interaction NU/L is increased due to the electrostatic interaction $\Delta_{\mathbf{q}}$.

Let us discuss the implications of Eq. (38). In the absence of electrostatic interaction we get due to U the usual phononic dispersion $\omega_{\mathbf{q}} = c_s \mathbf{q}$, where $c_s = \sqrt{NUK/L}$ is the speed of sound. This is the gapless Goldstone mode. To understand what is the fate of this mode we consider first a bulk superconductor for which the \mathbf{q} dependence of $\Delta_{\mathbf{q}} \propto 1/\mathbf{q}^2$ is canceled by the \mathbf{q} dependence of $\varepsilon_{\mathbf{q}} \propto \mathbf{q}^2$. Due to this cancellation we get a gapped mode with $\omega_{\mathbf{q}} \sim [\mathcal{R}^3/(\mathcal{L}^2 \ell)] \omega_p$. But for our one-dimensional ring $\Delta_{\mathbf{q}} \propto \ln(1/\mathbf{q})$, and therefore there is no such cancellation, and the phononic dispersion $\omega_{\mathbf{q}} = c_s \mathbf{q}$ is maintained. Still, c_s might become very large, leading to a gap due to a finite-size effect

$$\omega_{min} = c_s \frac{2\pi}{L} \sim \left(\frac{1}{L} \right) \left[\frac{\mathcal{R}^3}{\mathcal{L}^2 \ell} \right] \omega_p \quad (39)$$

This finite-size gap, compared with the effective plasma frequency, contains an enhancement factor that reflects the ratio between the volume of the cavity and the “volume” of the ring, and a $1/L$ suppression factor that reflects that the “gap” is due to a finite-size effect.

XI. SUMMARY AND DISCUSSION

We recall the quote of Einstein: “A scientific theory should be as simple as possible, but no simpler”. This perspective becomes of greater significance in the mesoscopic context. In this spirit, we were motivated to focus on a minimal model that combines SF and SC and and FR and MI regimes. The SF-SC transition is controlled by the generalized fine-structure-constant α , while the

transition to the MI phase is controlled by the interaction u .

Formally, in the absence of an EM mode, Φ can be interpreted as the scaled rotation velocity (Sagnac phase) of the ring. Experiments with such configurations have been realized in cold atom atomtronic experiments [28]. The optional interpretation of Φ as a dynamical variable that represents an EM mode, requires further attention [29]. Condensation of *charged* bosons is not a trivial matter [30, 31]. The idea actually predates BCS theory [32], and might be relevant to fermionic systems that feature a BCS-BEC crossover [33].

From an intellectual perspective, a model of charged bosons on a lattice constitutes a numerically accessible minimal model that allows exploration of fundamental questions regarding the relation between fully quantum and quasi-classical treatment of devices. We want to better understand the implication of treating a dynamical variable (here Φ) as a quantum degree of freedom rather than as a classical control parameter. Some aspects of this problem have been discussed in [34] regarding quantum mechanically driven adiabatic passage, but the present context looks more interesting in view of related quantum irreversibility study where Φ is the control parameter [35].

We have presented a semiclassical tomographic approach to study the SF-SC-FR-MI regions in the (U, α, ω_0, E) regime diagram of the circuit. Roughly speaking there are two dimensionless *classical* parameters u_L and w_L that control the emergence of SF and CD respectively, and an additional dimensionless *quantum* parameter γ_L that controls the MI transition. Illustrations that demonstrate the different spectral regions were provided, notably Fig.7b and Fig.8c. The observed spectral regions reflect the underlying valley structure of the energy landscape. The latter features Landau grooves that can support meta-stable condensates.

Due to the lattice nature of the BH ring, there is a vast crossover-region that mediates the MI transition, where quantum-chaos is pronounced, see Fig.6. We find that the EM-BH entanglement is rather correlated with the geometry of the energy surface, while ergodic measures probe the mixed-chaotic nature of the dynamics.

Finally we have addressed the Anderson-Higgs perspective of the Meissner effect, in the present mesoscopic context, using a device-oriented approach. The extra “mass” that is gained by the EM mode is a rather minor effect. More interesting is the electrostatic interaction that for bulk superconductor is responsible for the gap that is opened in the Goldstone excitation spectrum. For the one dimensional ring, depending on the geometry of the system, this interaction may lead to an enhanced gap due to a finite-size effect.

Acknowledgments – The research has been supported by the Israel Science Foundation, grant No.518/22.

Appendix A: Cavity mode

The Maxwell equation are derived from Hamiltonian whose conjugate coordinates are \mathcal{E} and $(1/c)\mathcal{A}$. Namely,

$$\mathcal{H} = \int d^3x \left[\frac{1}{8\pi} (\mathcal{E}^2 + (\nabla \times \mathcal{A})^2) - \frac{1}{c} \mathcal{J} \cdot \mathcal{A} \right] \quad (\text{A1})$$

where \mathcal{J} is a source. This Hamiltonian decomposes in a cavity into modes that are formally like Harmonic oscillators. Keeping a single mode we can use canonical variables $\Phi \equiv (1/c)\Phi_B$ and Q , where Φ_B is the magnetic flux through the ring, while Q is a canonically conjugate coordinate that reflects the electric field. Accordingly,

$$\mathcal{H} = \mathcal{H}_{EM}(Q, \Phi) - I_e(t)\Phi + \mathcal{U}_{ES} \quad (\text{A2})$$

where I_e is the current in the ring, and

$$\mathcal{H}_{EM} = \frac{1}{2C_e} Q^2 + \frac{c^2}{2L_e} \Phi^2 \quad (\text{A3})$$

and the electrostatic energy is

$$\mathcal{U}_{ES} = \frac{1}{8\pi} \int \mathcal{E}_{longitudinal}^2 d^3x \quad (\text{A4})$$

The equations of motion are

$$\dot{Q} = \frac{c^2}{L_e} \Phi - I_e(t) \quad (\text{A5})$$

$$\dot{\Phi} = -\frac{1}{C_e} Q \quad (\text{A6})$$

In the absence of a current source the free oscillations are with frequency ω_0 of Eq.(2) that reflects the linear size of the cavity.

Let us elaborate how L_e and C_e are determined in practice. Disregarding the BH ring, one can choose natural coordinates (Q_{EM}, Φ_{EM}) that describe the EM mode such that $C_{EM} \sim L_{EM}$ equal the linear size of the cavity. The cavity and the ring are formally coupled circuits, with mutual inductance $L_\perp \sim \mathcal{L}$ that reflects the linear size of the embedded ring. The circuit equation $\Phi_{EM} = L_{EM}\dot{Q}_{EM} + L_\perp I_e$ implies that the interaction term is $-(L_\perp/L_{EM})I_e\Phi_{EM}$. We identify $\Phi = (L_\perp/L_{EM})\Phi_{EM}$ as the flux of the EM mode via the ring. It follows that the inductance of the EM mode is $L_e = L_\perp^2/L_{EM}$. We conclude that L_e is typically much smaller than the linear size of the ring.

Appendix B: Cavity with SQUID

The Hamiltonian for cavity that includes a driving source and a SQUID-type ring can be written as [29]

$$\mathcal{H} = \mathcal{H}_{EM} - I_{ext}(t)\Phi + \mathcal{H}_{ring} \quad (\text{B1})$$

The ring is a chain of Josephson junctions (weak links) in series, namely,

$$\mathcal{H}_{ring} = \frac{E_C}{2} \sum_{j=1}^L \mathbf{n}_j^2 - E_J \sum_j \cos \left(\varphi_j - \varphi_{j-1} - \frac{e\Phi}{L} \right) \quad (\text{B2})$$

analogous to Eq.(8). We use the notation

$$\Phi_{ext} = \frac{1}{c^2} L_e I_{ext} \quad (\text{B3})$$

and define $\phi \equiv e\Phi - e\Phi_{ext}$ as the flux coordinate of the ring. Expressing \mathcal{H}_{EM} with ϕ as in Eq.(8), this allows us to get rid of the source term in Eq.(B1), and the price is $e\Phi \mapsto \phi + \phi_{ext}$ in Eq.(B2). It follows that the total flux inside the ring is

$$\phi_{in} = \phi_{ext} + \phi \quad (\text{B4})$$

For very large L , taking the continuum limit and using quadratic approximation for the cosines, one concludes that the ϕ coordinate experiences the potential

$$V(\phi) = \frac{K_e}{2} \phi^2 + \frac{K_L}{2} (\phi + \phi_{ext} - 2\pi m)^2 \quad (\text{B5})$$

where m is integer that reflects the winding number of the phase. The first term of $V(\phi)$ originates from \mathcal{H}_{EM} while the second term from \mathcal{H}_{ring} . The definition of the coefficients is implied, namely, $K_e = (c/e)^2/L_e$ and $K_L = E_J/L^2$. For $e = 0$ the minimum of $V(\phi)$ is at $\phi = 0$, meaning that the ring does not respond to the external source (no screening). For finite e we get

$$\phi_{in} = \frac{\phi_{ext}}{1+w} + \frac{2\pi m}{1+w^{-1}} \quad (\text{B6})$$

where $w = K_L/K_e$ is the dimensionless screening parameter. In the absence of screening ($w = 0$) we get the triviality $\phi = \phi_{ext}$, while for very large w we get flux quantization. One observes that w of the SQUID is the same as the w_L that has been defined in Eq.(12).

Appendix C: Meissner effect for a thick ring

Consider a cylindrical ring of radius R that has finite thickness d . We solve the equation of the magnetic field $B(r)$ within $R < r < (R+d)$, assuming $d \ll R$. To simplify the geometry we assume that the height of the cylinder is very large. Given that the density of the superconducting carries is n_s , the London penetration distance is defined as

$$\lambda = \left(4\pi \frac{e^2}{Mc^2 n_s} \right)^{-1/2} \quad (\text{C1})$$

where M is the mass of the particles. We can regard the thick ring as composed of very thin cylindrical rings. The radius r ring has thickness dr , and encloses a flux $\Phi(r)$.

Hence, by the London equation, it carries a current density

$$J(r) = \left[\left(\frac{1}{2\pi r} \right) \frac{n_s}{M} \right] [2\pi m - e\Phi(r)] \quad (\text{C2})$$

By geometry the flux satisfies

$$\frac{d\Phi}{dr} = (2\pi r) \frac{e}{c} B(r) \quad (\text{C3})$$

while Ampere law is

$$\frac{dB}{dr} = -\frac{4\pi}{c} e J(r) \quad (\text{C4})$$

Thus we get the equation

$$\frac{d^2\Phi}{dr^2} = \frac{1}{\lambda^2} [e\Phi(r) - 2\pi m] \quad (\text{C5})$$

The solution for $\Phi(x)$ is $2\pi m$ plus a linear combination of $\cosh(x/\lambda)$ and $\sinh(x/\lambda)$, where $x = r - R$. The

solution for $B(x)$ is obtained by taking the derivative. The formal boundary conditions are: $\Phi(0) = \Phi_{\text{in}}$ and $(e/c)B(0) = \Phi_{\text{in}}/(\pi R^2)$ and $(e/c)B(d) = \Phi_{\text{ext}}/(\pi R^2)$. From that we can get the result:

$$e\Phi_{\text{in}} = \frac{e\Phi_{\text{ext}}}{\cosh(\frac{d}{\lambda}) + \frac{R}{2\lambda} \sinh(\frac{d}{\lambda})} + \frac{2\pi m}{1 + \frac{2\lambda}{R} \coth(\frac{d}{\lambda})} \quad (\text{C6})$$

For $d \gg \lambda$ the first term is exponentially suppressed, and one obtains $e\Phi_{\text{in}} \approx 2\pi m$, which is the usual statement of the Meissner effect for a thick ring. For a thin ring $d \ll \lambda$ the result becomes the same as Eq.(B6) with

$$w = \frac{\mathcal{L}d}{4\pi\lambda^2} \sim \frac{e^2 N}{c^2 M} \left[\frac{1}{\mathcal{L}_{\parallel}} \right] \quad (\text{C7})$$

where $\mathcal{L} = 2\pi R$ and \mathcal{L}_{\parallel} is the height of the cylindrical ring. Eq.(C1) has been used with $n_s = N/(\mathcal{L}_{\parallel}\mathcal{L}d)$. The w of Eq.(C7) should be compared with the w_L of Eq.(12). In the latter the same expression appears but with $1/\mathcal{R}$ in the square brackets. Note however that the $\lambda \propto \mathcal{R}^{3/2}$ in Eq.(12) is merely a formal notation, unlike the $\lambda \propto (\mathcal{L}_{\parallel}\mathcal{L}d)^{1/2}$ of Eq.(C7).

[1] A.J. Leggett, *Bose-Einstein condensation in the alkali gases: Some fundamental concepts*, Rev. Mod. Phys. 73, 307 (2001)

[2] M. Greiner, O. Mandel, T. Esslinger, T.W. Hansch, I. Bloch, *Quantum phase transition from a superfluid to a Mott insulator in a gas of ultracold atoms*, Nature volume 415, 39 (2002)

[3] O. Morsch and M. Oberthaler, *Dynamics of Bose-Einstein condensates in optical lattices*, Rev. Mod. Phys. 78, 179 (2006)

[4] I. Bloch, J. Dalibard, and W. Zwerger, *Many-body physics with ultracold gases*, Rev. Mod. Phys. 80, 885 (2008)

[5] A.J. Leggett, *Superfluidity*, Rev. Mod. Phys. 71, S318 (1999)

[6] A.J. Leggett, *The Penrose-Onsager-Yang Approach to Superconductivity and Superfluidity*, chapter in "Dialogues Between Physics and Mathematics", Editors: Mo-Lin Ge, Yang-Hui He (Springer 2022)

[7] P.W. Anderson, *Coherent Excited States in the Theory of Superconductivity: Gauge Invariance and the Meissner Effect*, Phys. Rev. 110, 827 (1958)

[8] P.W. Anderson, *Plasmons, Gauge Invariance, and Mass*, Phys. Rev. 130, 439 (1963)

[9] P.W. Anderson, *Higgs, Anderson and all that*, Nature Physics 11, 93 (2015)

[10] K.V. Grigorishin, *Extended Time-Dependent Ginzburg-Landau Theory*, J.Low.Temp.Phys. 203, 262 (2021)

[11] T. D. Kuhner and H. Monien, *Phases of the one-dimensional Bose-Hubbard model*, Phys. Rev. B 58, R14741 (1998)

[12] T. Sowinski, *Exact diagonalization of the one-dimensional Bose-Hubbard model with local three-body interactions*, Phys. Rev. A 85, 065601 (2012)

[13] S. Ejima, H. Fehske, F. Gebhard, K. zu Munster, M. Knap, E. Arrigoni, W. von der Linden, *Characterization of Mott-insulating and superfluid phases in the one-dimensional Bose-Hubbard model*, Phys. Rev. A 85, 053644 (2012)

[14] M. Chuchem, K. Smith-Mannschott, M. Hiller, T. Kottos, A. Vardi, D. Cohen, *Quantum dynamics in the bosonic Josephson junction*, Phys. Rev. A 82, 053617 (2010)

[15] T. Opatrny, L. Richterek and M. Opatrny, *Analogy of the classical Euler top with a rotor to spin squeezing and quantum phase transitions in a generalized Lipkin-Meshkov-Glick model*, Scientific Reports 8, 1984 (2018)

[16] L. Pausch, E.G. Carnio, A. Rodriguez, A. Buchleitner, *Chaos and Ergodicity across the Energy Spectrum of Interacting Bosons*, Phys. Rev. Lett. 126, 150601 (2021)

[17] L. Pausch, A. Buchleitner, E.G. Carnio, A. Rodriguez, *Optimal route to quantum chaos in the Bose-Hubbard model*, J. Phys. A: Math. Theor. 55 324002 (2022)

[18] Y. Winsten, D. Cohen, *Quantum tomography of the superfluid-insulator transition for a mesoscopic atomtronic ring*, Phys. Rev. A 112, 013305 (2025)

[19] A. Smerzi, A. Trombettoni, P.G. Kevrekidis, and A.R. Bishop, *Dynamical Superfluid-Insulator Transition in a Chain of Weakly Coupled Bose-Einstein Condensates*, Phys. Rev. Lett. 89, 170402 (2002)

[20] A. R. Kolovsky, *Semiclassical quantization of the Bogoliubov spectrum*, Phys. Rev. Lett. 99, 020401 (2007).

[21] M. Hiller, T. Kottos, and T. Geisel, *Wave-packet dynamics in energy space of a chaotic trimeric Bose-Hubbard system*, Phys. Rev. A 79, 023621 (2009)

[22] H. Hennig and R. Fleischmann, *Nature of self-localization of Bose-Einstein condensates in optical lattices*, Phys. Rev. A 87, 033605 (2013).

- [23] A. Richaud and V. Penna, *Phase separation can be stronger than chaos*, New J. Phys. 20 105008 (2018)
- [24] G. Arwas, A. Vardi, D. Cohen, *Superfluidity and Chaos in low dimensional circuits*, Scientific Reports 5, 13433 (2015)
- [25] G. Arwas, D. Cohen, *Superfluidity in Bose-Hubbard circuits*, Phys. Rev. B 95, 054505 (2017)
- [26] G. Nakerst and M. Haque, *Chaos in the three-site Bose-Hubbard model: Classical versus quantum*, Phys. Rev. E 107, 024210 (2023)
- [27] A. Vardi, D. Cohen, *Quantum thermalization and the route to ergodicity*, (arXiv 2025)
- [28] L. Amico et al., *Roadmap on atomtronics: State of the art and perspective*, AVS Quantum Science 3, 039201 (2021).
- [29] *New Trends and Platforms for Quantum Technologies*, Editors: Ramon Aguado, Roberta Citro, Maciej Lewenstein, Michael Stern (Springer 2024)
- [30] I.V. Lukin, A.G. Sotnikov, Yu.V. Slyusarenko, *Aspects of Bose-Einstein condensation in a charged boson system over the dielectric surface*, Physics Letters A 417, 127695 (2021)
- [31] Shun-ichiro Koh, *Meissner effect in a charged Bose gas with short-range repulsion*, Phys. Rev. B 68, 144502 (2003)
- [32] M.R. Schaefroth, *Superconductivity of a Charged Ideal Bose Gas*, Phys. Rev. 100, 463 (1955)
- [33] Q. Chen, Z. Wang, R. Boyack, S. Yang, and K. Levin, *When superconductivity crosses over: From BCS to BEC*, Rev. Mod. Phys. 96, 025002 (2024)
- [34] A.V. Varma, D. Cohen, *Quantum measurement of work in mesoscopic systems*, (arXiv 2025)
- [35] Y. Winsten, D. Cohen, *Quantum irreversibility of quasistatic protocols for finite-size quantized systems*, Phys. Rev. A 107, 052202 (2023)